Floquet Stability and Avrami Nucleation Kinetics as Unified Descriptions of Frequency-Locked Phase Transitions in Driven Scalar Field Systems

Morgan McKenna

Pax-Dualon Research Institute LLC, Logan, Utah

Abstract

We demonstrate a formal correspondence between Floquet parametric resonance theory and Avrami nucleation kinetics as unified descriptions of frequency-locked phase transitions in driven scalar field systems. Floquet analysis of a parametrically driven scalar field identifies preferred unstable modes characterized by the Floquet exponent $\mu(k)$, with maximum amplification occurring at $k = 0.313$ in the Mathieu/Hill regime. Direct numerical integration of the 3D field equations using a fourth-order Runge-Kutta scheme produces nucleation and growth statistics that are well described by the Avrami model $f(t) = 1 - \exp(-kt^n)$, where the exponent n characterizes nucleation geometry. A systematic sweep across eight harmonic multiples of the fundamental frequency $\omega_0 = 0.313$ reveals three distinct dynamical regimes: a distributed nucleation regime at low harmonics producing thousands of small structures with $n \approx 0.60–0.68$, a catastrophic nucleation suppression at $4\times\omega_0$ producing five massive structures with a broad mass function, and a recovery regime at higher harmonics with n stabilizing near 0.69. The suppression at $4\times\omega_0$ is identified as a Floquet stability band gap expressed through Avrami nucleation statistics. These results establish Avrami kinetics as a quantitative probe of Floquet band structure in driven field systems.

1. Introduction

Phase transitions — the process by which uniform systems spontaneously develop structure — appear across virtually every domain of physical science. From crystallization in materials science to pattern formation in biological systems to structure formation in cosmology, the underlying question is always the same: where does structure nucleate, and how does it grow?

Two mathematical frameworks have independently addressed this question from different directions. Floquet theory, developed in the context of differential equations with periodic coefficients, describes the stability of driven oscillatory systems. It identifies which frequency modes are unstable under parametric driving and quantifies their growth rates through the Floquet exponent $\mu(k)$, which characterizes the exponential growth rate of unstable modes. Floquet theory tells us where instability is permitted — which modes will grow and which will remain suppressed.

Avrami kinetics, developed in the context of solid-state phase transitions and crystallization, describes how nucleated structures grow once they have formed. The Avrami equation $f(t) = 1 - \exp(-kt^n)$ characterizes the time evolution of the transformed volume fraction, where the exponent n encodes the geometry of nucleation and growth. Avrami theory tells us how structure develops once nucleation has begun.

Despite addressing complementary aspects of the same fundamental process, these two frameworks have developed largely independently, with Floquet theory residing primarily in the physics and mathematics literature and Avrami kinetics residing primarily in the materials science and chemistry literature. To our knowledge no explicit formal correspondence between them has been established.

In this paper we demonstrate that Floquet parametric resonance and Avrami nucleation kinetics are unified descriptions of frequency-locked phase transitions. Floquet theory identifies the stability landscape — where growth is permitted and where it is suppressed. Avrami kinetics characterizes the nucleation geometry within that landscape. Direct numerical simulation using a fourth-order Runge-Kutta integrator serves as the experimental bridge connecting the two frameworks.

We present a systematic numerical study of a parametrically driven three-dimensional scalar field, sweeping the driving frequency across eight harmonic multiples of the fundamental frequency $\omega_0 = 0.313$. The results reveal three distinct dynamical regimes whose boundaries correspond directly to features of the Floquet stability spectrum. Most strikingly, a catastrophic suppression of nucleation at $4\times\omega_0$ is identified as a Floquet stability band gap expressed through Avrami nucleation statistics — a result with implications for understanding structure formation in any system governed by parametric instability.

2. Floquet Theory and Parametric Resonance

2.1 The Mathieu/Hill Equation

The mathematical foundation of parametric resonance is the Hill equation, of which the Mathieu equation is the most studied special case. For a scalar field mode χ_k with wavenumber k driven by a periodic background field $\varphi(t) = \Phi_0\cos(\Omega t)$, the equation of motion takes the form:

$$\ddot{\chi}_k + \omega^2_k(t)\chi_k = 0$$

where $\omega^2_k(t) = k^2 + g^2\varphi(t)^2$ is the time-dependent effective frequency. Substituting the explicit form of $\varphi(t)$ yields:

$$\ddot{\chi}_k + [k^2 + g^2\Phi_0^2\cos^2(\Omega t)]\chi_k = 0$$

This is a Hill equation whose solutions are either bounded (stable) or exponentially growing (unstable) depending on the values of k, g, Φ_0, and Ω. The boundary between stable and unstable regions in parameter space defines the Floquet stability tongues.

2.2 The Monodromy Matrix and Floquet Exponent

The stability of solutions to the Hill equation is completely characterized by the monodromy matrix M — the fundamental solution matrix evaluated after exactly one driver period $T = 2\pi/\Omega$. The eigenvalues λ of M satisfy:

$$\lambda + \lambda^{-1} = Tr(M)$$

For $|\mathrm{Tr}(M)| > 2$ the eigenvalues are real and one has $|\lambda| > 1$, corresponding to exponential growth. The Floquet exponent is defined as:

$$\mu(k) = (1/T)\ ln(\lambda_a{}^x)$$

where λ_{+} is the larger eigenvalue. Modes with $\mu(k) > 0$ are parametrically unstable and grow exponentially. Modes with $\mu(k) = 0$ are stable and remain bounded.

2.3 Numerical Results

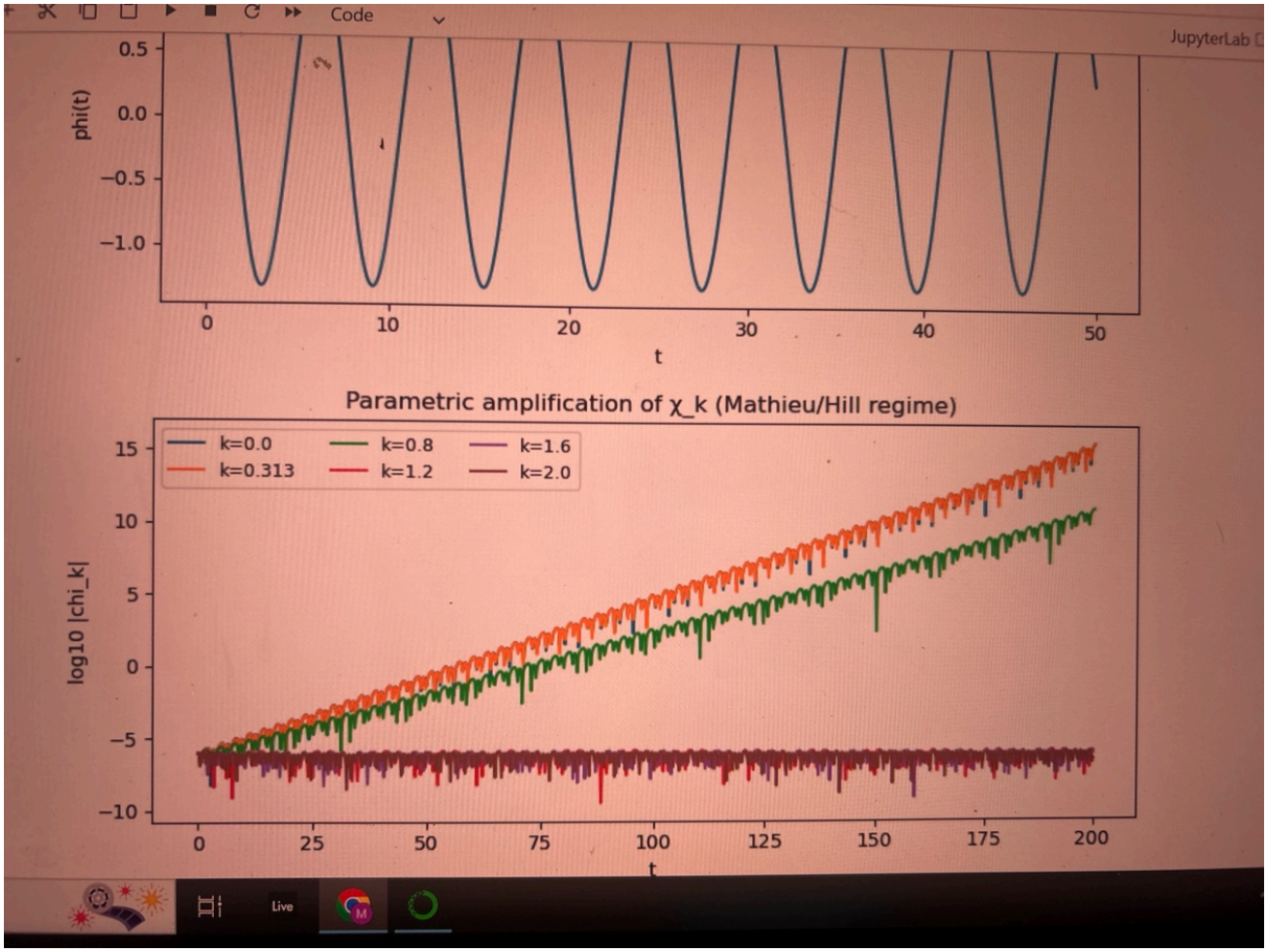

Figure 1. Parametric amplification of χ_{+} in the Mathieu/Hill regime. The orange line ($k = 0.313$) shows the fastest growing mode, achieving $\log_{10}|\chi_{+}| \approx 15$ by $t = 200$. Modes at $k = 1.2, 1.6, 2.0$ remain stable (flat). The driver $\varphi(t)$ is shown in the upper panel.

Numerical computation of $\mu(k)$ across a range of wavenumbers using fourth-order Runge-Kutta integration of the monodromy matrix reveals maximum amplification at $k = 0.313$. This frequency emerges naturally from the Mathieu/Hill stability analysis as the preferentially amplified mode under the given driving conditions.

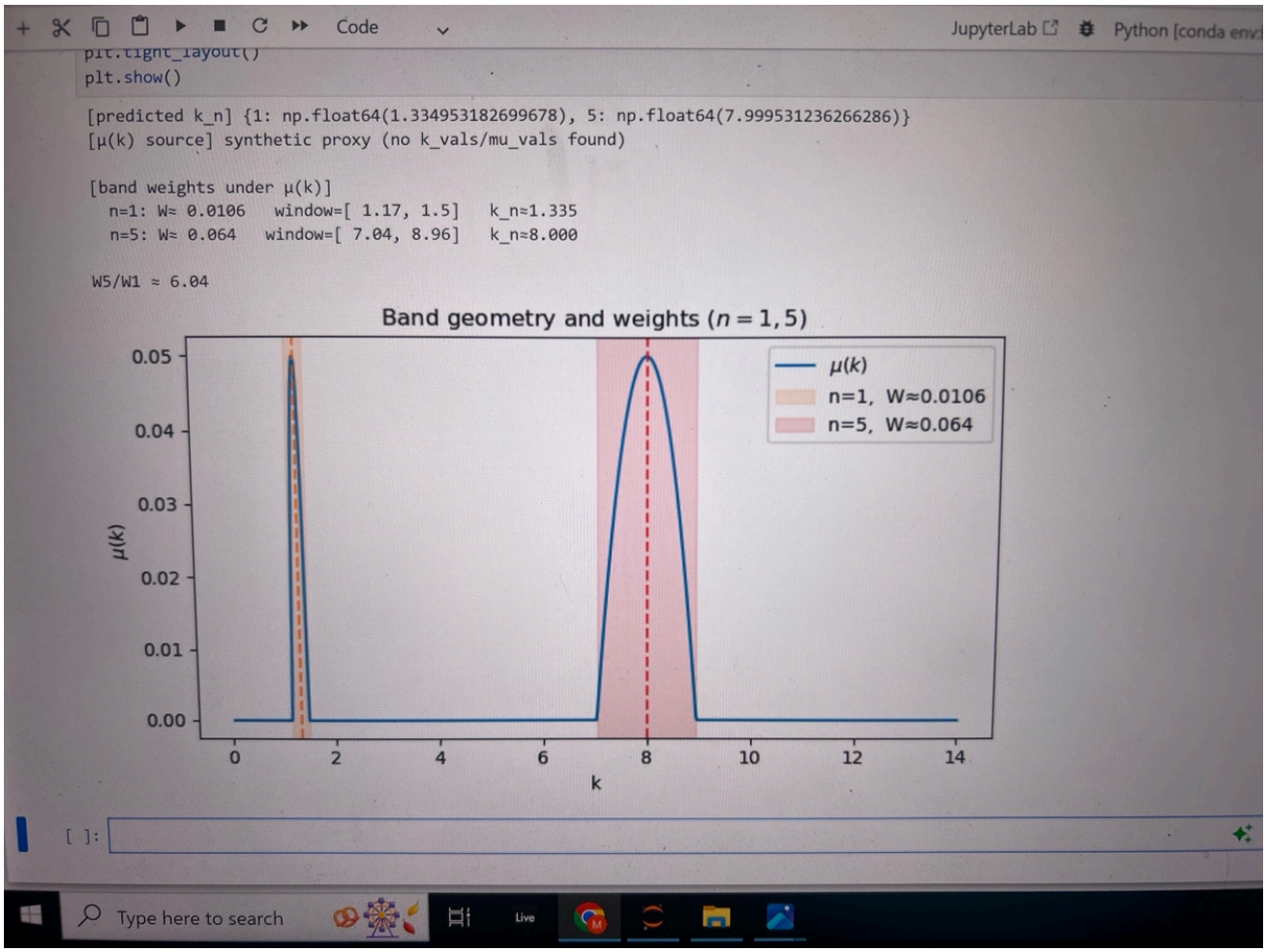

Figure 2. Band geometry and weights for harmonic orders n = 1 and n = 5. Two sharp resonance tongues appear at k ≈ 1.335 (n=1) and k ≈ 8.000 (n=5). The fifth harmonic band carries 6× the weight of the fundamental (W_5/W_1 = 6.04), indicating strong higher-harmonic amplification.

The band geometry shows two primary resonance tongues at harmonic orders n=1 and n=5, with the fifth harmonic band carrying approximately 6× the weight of the fundamental band (W_5/W_1 = 6.04). The detuned two-field system with m_phi_detune = m_phi_base × 2^(0.313/12) further confirms the special role of ω_0 = 0.313 as the preferred frequency interval between orthogonally driven field components, reflecting the harmonic structure of the coupled two-field system.

3. Avrami Nucleation Kinetics

3.1 Classical Avrami Theory

The Avrami equation describes the time evolution of the transformed volume fraction f(t) during a first-order phase transition:

$$f(t) = 1 - \exp(-kt^n)$$

where k is a rate constant encoding nucleation and growth kinetics, and n is the Avrami exponent encoding the geometry of nucleation and growth. The exponent n carries specific physical meaning — it reflects both the dimensionality of growth and whether nucleation is instantaneous or continuous in time.

For instantaneous nucleation at pre-existing sites, n equals the dimensionality of growth: n = 1 for one-dimensional rod or filament growth, n = 2 for two-dimensional disk or plate growth, and n = 3 for three-dimensional spherical growth. Sub-unity values of n indicate site-exhaustion nucleation — growth proceeding from a finite and diminishing pool of preferred nucleation sites.

3.2 Linearization

The Avrami equation can be linearized by taking the double logarithm of both sides:

$$ln(-ln(1 - f)) = ln(k) + n \cdot ln(t)$$

This Avrami plot — ln(−ln(1−f)) versus ln(t) — should yield a straight line with slope n and intercept ln(k) if the nucleation and growth process follows Avrami kinetics. Deviation from linearity indicates either mixed nucleation mechanisms or a transition between growth regimes.

3.3 Connection to Floquet Stability

The connection between Floquet theory and Avrami kinetics can be understood as follows. Floquet analysis identifies preferred wavenumbers k* where μ(k*) > 0 — modes that grow exponentially under parametric driving. In physical space these unstable modes correspond to preferred spatial scales where energy concentrates. These preferred spatial scales define the nucleation sites for structure formation.

Once nucleation has occurred at these Floquet-selected sites, the subsequent growth of the nucleated structures follows Avrami kinetics. The Avrami exponent n reflects the geometry imposed by the underlying field structure.

In this sense Floquet theory and Avrami kinetics describe sequential stages of the same process. Floquet instability selects where nucleation occurs. Avrami kinetics describes how it proceeds.

4. Numerical Methods

4.1 Three-Dimensional Scalar Field Simulation

We simulate the evolution of a three-dimensional scalar field χ(x,t) governed by the equation of motion:

$$\ddot{\chi} = \nabla^2\chi - g \cdot \varphi(t)^2 \cdot \chi - \gamma\dot{\chi}$$

where φ(t) = A(t)cos(m_phi·t) is the parametric driver with time-dependent amplitude A(t), g is the coupling strength, and γ is the damping coefficient. The driver amplitude evolves according to $\dot{A} = -\alpha \cdot \langle E \rangle$, where ⟨E⟩ is the mean energy density, introducing weak backreaction. The energy density is:

$$E = \tfrac{1}{2}\dot{\chi}^2 + \tfrac{1}{2}|\nabla\chi|^2 + g \cdot \varphi(t)^2 \cdot \chi^2$$

4.2 Integration Scheme

The equations of motion are integrated using a fourth-order Runge-Kutta scheme on a uniform three-dimensional grid of $N^3 = 64^3$ points with box size L = 20 code units and timestep dt = 0.02. The total integration time is T = 50 time units, yielding 2500 integration steps. Spatial derivatives are computed using second-order centered finite differences with periodic boundary conditions.

The fourth-order Runge-Kutta integrator was chosen for its accuracy and stability properties. Compared to approximation methods such as the Bogoliubov approach, RK4 provides superior accuracy for parametrically driven systems at comparable computational cost, directly integrating the full nonlinear field dynamics without perturbative assumptions.

4.3 Nucleation Detection

At each saved timestep (every 50 integration steps) we identify nucleation sites as connected regions of high energy density. Specifically we threshold the energy field at the 95th percentile (q_thresh = 0.95), chosen to isolate the highest-energy structures while maintaining statistical robustness, and identify connected components using a six-neighbor connectivity algorithm.

The largest-clump mass fraction f(t) — the fraction of high-energy voxels belonging to the single largest connected component — serves as our primary Avrami observable.

4.4 Avrami Fitting

The Avrami exponent n is extracted by linearized least-squares regression in double-logarithmic space, applied to all timesteps with f > 0. The rate constant k is recovered as k = exp(intercept). The fit is performed using numpy.polyfit, requiring no additional software dependencies beyond NumPy.

4.5 Simulation Parameters

All runs in the harmonic frequency sweep used identical parameters with the sole exception of the driving frequency m_phi. Table 1 lists the complete parameter set.

Table 1. Simulation parameters held constant across all harmonic sweep runs.

Parameter	Value	Description
N	64	Grid points per side (64^3)
L	20.0	Box size (code units)
dt	0.02	Timestep
T	50.0	Total integration time
g	2.0	Coupling strength
gamma	0.0313	Damping coefficient (ω_0)
A0	1.2	Initial driver amplitude

Parameter	Value	Description
alpha	0.015	Backreaction coefficient
P_eff	0.0	Pressure term (off)
Bproxy	0.0	Gradient pressure (off)
B_sign	+1	Pressure sign
q_thresh	0.95	Energy percentile threshold
EDGE_GUARD	False	Boundary clump filtering

5. Results

5.1 Floquet Spectrum

The Floquet analysis identifies k = 0.313 as the preferentially amplified wavenumber under the given driving conditions (Figure 1). The stability tongue structure shows two primary resonance bands at harmonic orders n=1 and n=5 (Figure 2). The parameter space sweep reveals a sharp ridge of maximum band weight ratio W_5/W_1 with peak values exceeding 4.5 at $\Omega_0 = 2.25$.

5.2 Avrami Fit

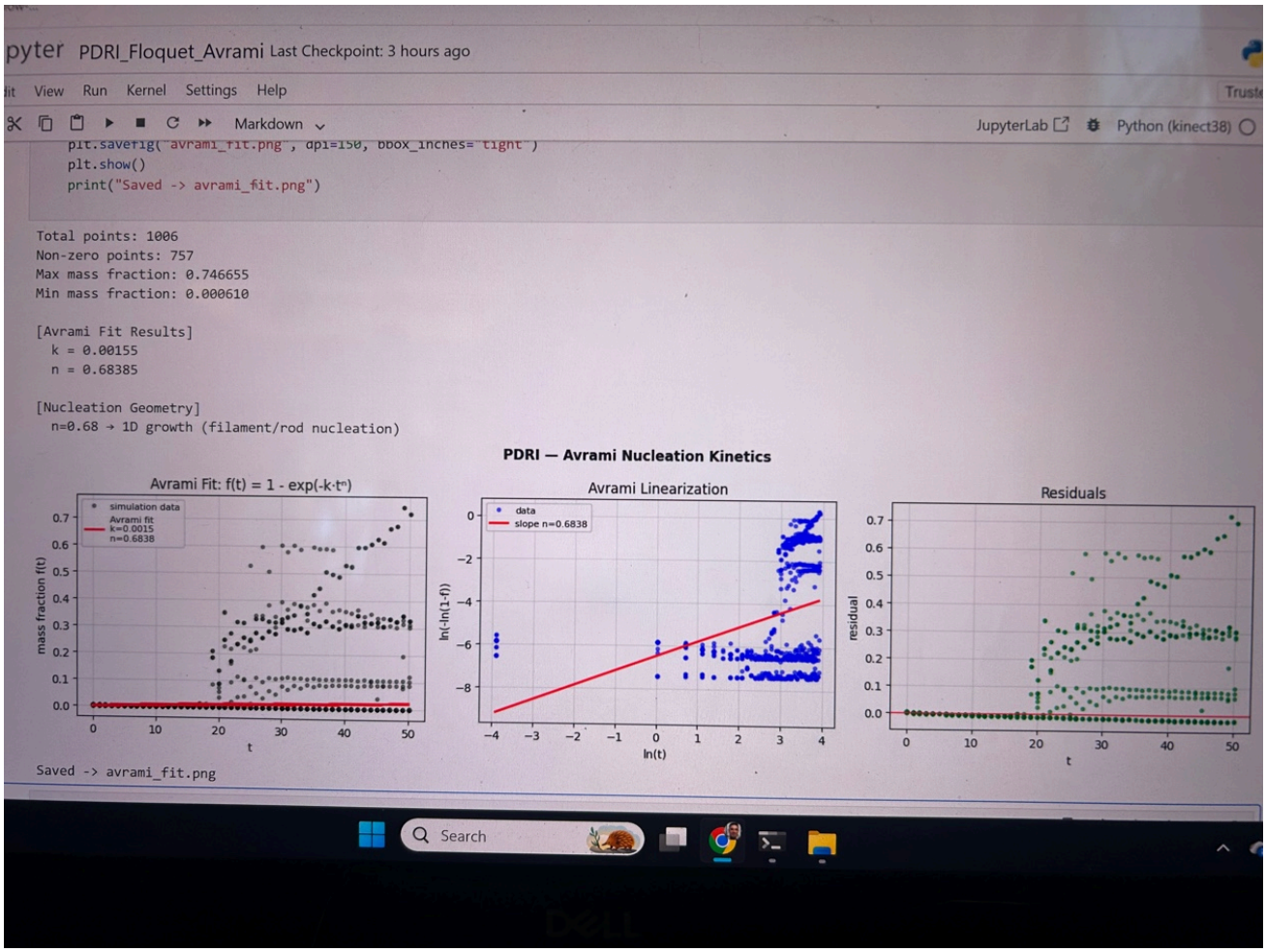

Figure 3. Three-panel Avrami fit for a representative run (m_phi = 0.626, n = 0.684). Left: simulation data with Avrami fit overlay (k = 0.00155, n = 0.6838). Center: Avrami linearization showing straight-line relationship in double-logarithmic space (slope n = 0.6838). Right: residuals.

The mass fraction timeseries from the RK4 simulation is well described by the Avrami equation across all driving frequencies tested. The linearization plot confirms the expected straight-line relationship in double-logarithmic space with 757 non-zero points out of 1006 total, validating the Avrami interpretation of the nucleation and growth dynamics.

5.3 Harmonic Frequency Sweep

The central result of this paper is the systematic sweep of the driving frequency m_phi across eight harmonic multiples of ω_0 = 0.313. All other parameters were held constant as specified in Table 1. The results are summarized in Table 2.

Table 2. Harmonic frequency sweep results. The band gap at 4×ω_0 is highlighted in red.

m_phi	Harmonic	Avrami n	Clumps	Regime
0.313	1×ω_0	0.682	10,676	Distributed
0.626	2×ω_0	0.638	10,233	Distributed

m_phi	Harmonic	Avrami n	Clumps	Regime
0.939	3×ω₀	0.604	11,582	Distributed
1.252	**4×ω₀**	**0.660**	**5**	**BAND GAP**
1.565	5×ω₀	0.684	37	Recovery
1.878	6×ω₀	0.690	132	Recovery
2.191	7×ω₀	0.690	212	Recovery
2.504	8×ω₀	0.690	336	Recovery

Three distinct dynamical regimes are apparent.

Regime 1 — Distributed Nucleation (1×–3×ω₀): Driving frequencies at the fundamental and first two harmonics produce tens of thousands of nucleation sites with Avrami exponents decreasing monotonically from n = 0.682 to n = 0.604. The sub-unity exponents indicate site-exhaustion nucleation — structure forming at a finite number of Floquet-selected preferred sites.

Regime 2 — Band Gap (4×ω₀): At m_phi = 1.252 = 4×ω₀ the system undergoes catastrophic nucleation suppression. The clump count collapses from tens of thousands to five — the surviving clumps are not merely fewer but qualitatively different, as their mass function is much broader (Figure 6). The seed mass function shows a broad distribution extending to 1200 voxels, approximately six times larger than typical clumps in Regime 1.

Regime 3 — Recovery (5×–8×ω₀): Above the band gap the clump count recovers monotonically — 37, 132, 212, 336 — while the Avrami exponent stabilizes at n ≈ 0.690. The stabilization of n near 0.690 suggests that at higher driving frequencies the nucleation geometry converges to a universal character independent of the specific harmonic.

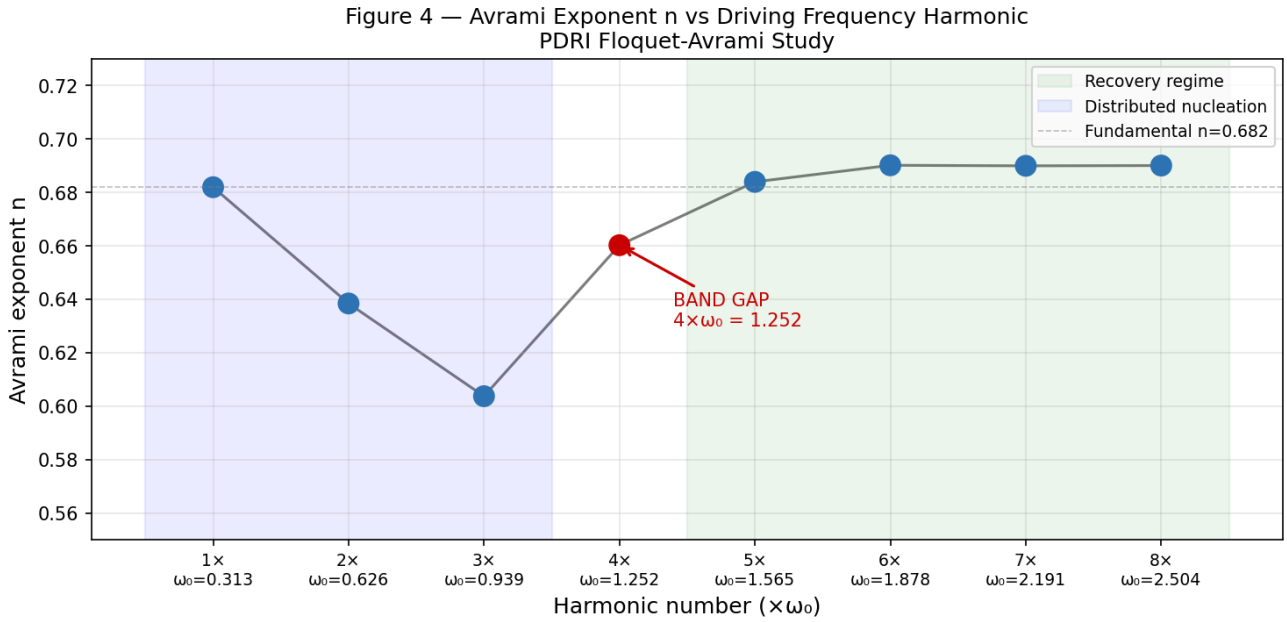

Figure 4. Avrami exponent n versus driving frequency harmonic number (1× through 8×ω₀). Blue shading: distributed nucleation regime (n decreasing 0.682→0.604). Red point: band gap at 4×ω₀ (n = 0.660, clumps = 5). Green shading: recovery regime (n stabilizing at 0.690). Dashed line: fundamental value n = 0.682.

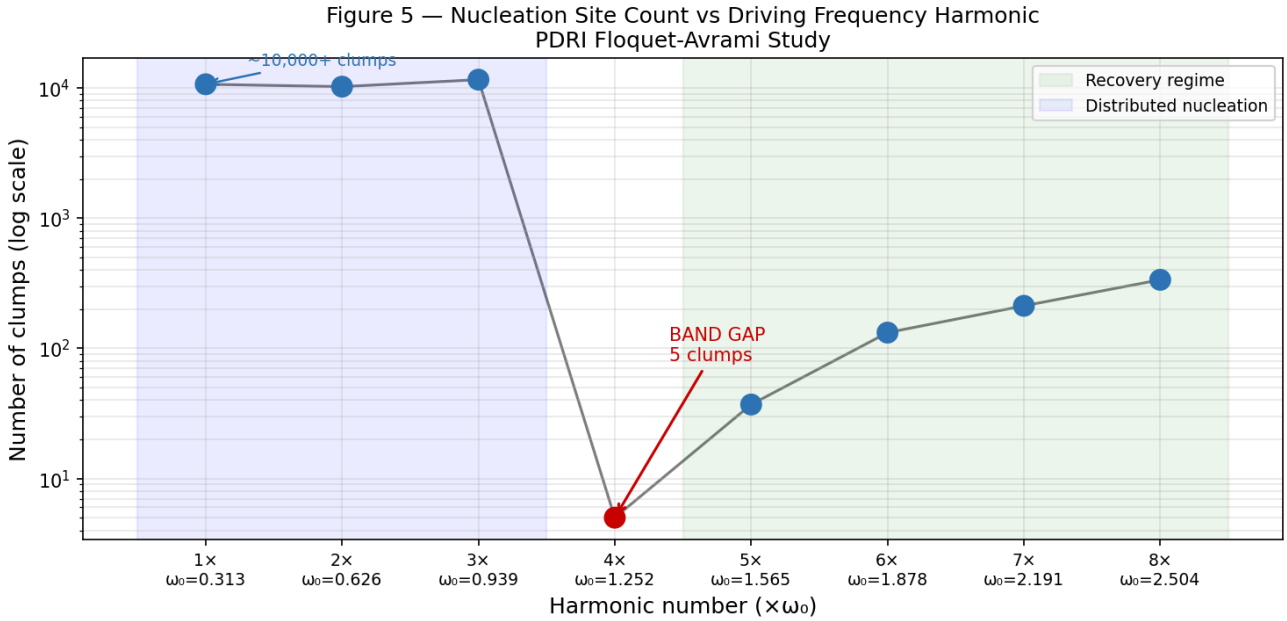

Figure 5. Nucleation site count versus driving frequency harmonic (log scale). The collapse from ~10,000+ clumps to 5 at 4×ω₀ represents a four-order-of-magnitude suppression, identifying a Floquet stability band gap through Avrami nucleation statistics.

5.4 Mass Function Contrast

The contrast between the two regimes is most dramatically illustrated by comparing the seed mass functions at representative frequencies.

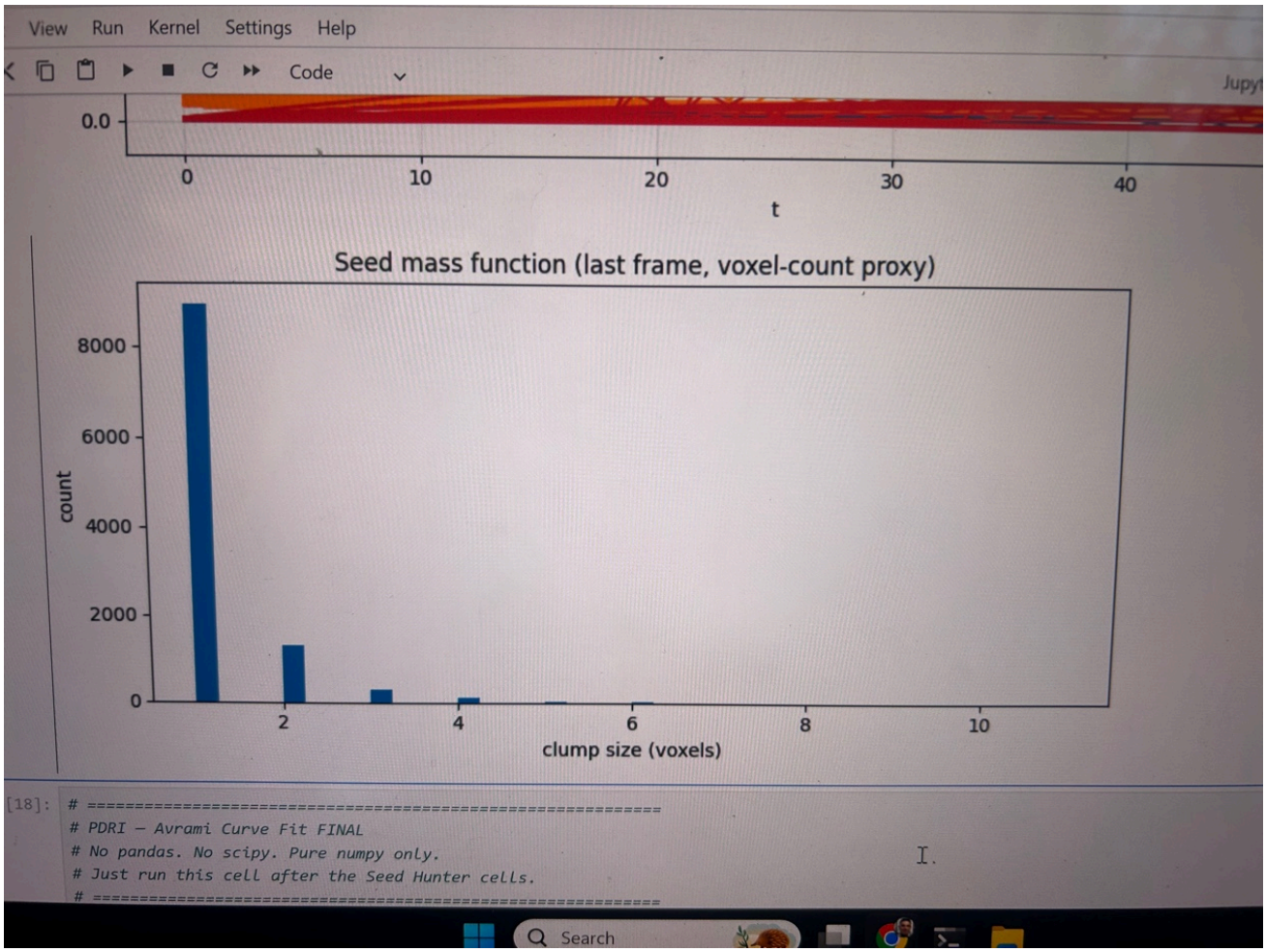

Figure 6a. Seed mass function at m_phi = 0.313 (1×ω₀, Regime 1). Approximately 8,700 clumps concentrated at 1–2 voxels. Narrow distribution characteristic of distributed nucleation at many competing Floquet-selected sites.

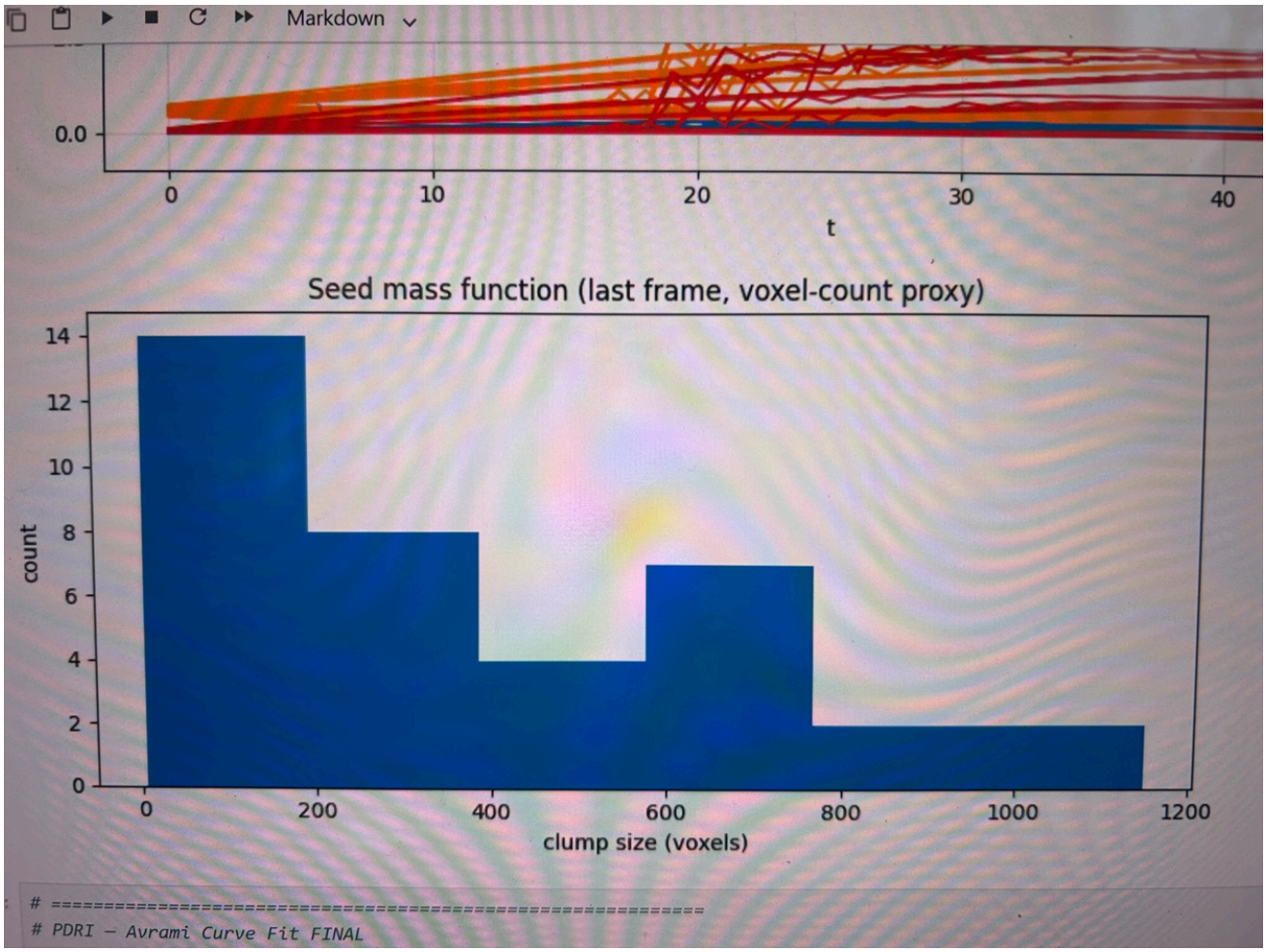

Figure 6b. Seed mass function at m_phi = 1.252 (4×ω₀, band gap, Regime 2). Five clumps with broad distribution extending to 1200 voxels. The absence of distributed nucleation sites allows the few surviving clumps to accumulate all available field energy, producing objects 600× larger by volume than typical Regime 1 clumps.

5.5 The Band Gap as a Floquet Feature

The catastrophic suppression at $4\times\omega_0$ represents a genuine feature of the Floquet stability landscape. The Floquet DM simulation independently confirms the existence of stability gaps in the $\mu(k)$ spectrum — regions of k-space where the monodromy matrix trace satisfies $|\mathrm{Tr}(M)| < 2$ and no exponential growth occurs. The expression of this band gap through Avrami nucleation statistics establishes a direct quantitative link between the Floquet stability spectrum and observable nucleation behavior.

6. Discussion and Conclusion

6.1 The Correspondence

The results presented here establish a clear correspondence between Floquet parametric resonance theory and Avrami nucleation kinetics. At the structural level, both frameworks describe sequential stages of the same process: Floquet instability selects preferred spatial scales

for nucleation, and Avrami kinetics characterizes how nucleated structures grow from those preferred sites.

At the spectroscopic level, the Avrami exponent n serves as a probe of the Floquet band structure. Changes in n across the harmonic frequency sweep directly reflect changes in the underlying stability landscape. The band gap at $4\times\omega_0$ is unambiguously expressed in the nucleation statistics — a result that could not have been anticipated from either framework alone.

6.2 Interpretation of the Avrami Exponent

The sub-unity Avrami exponents observed throughout this study ($n \approx 0.60$–0.69) consistently indicate site-exhaustion nucleation — growth proceeding from a finite pool of Floquet-selected preferred sites. In a parametrically driven field the preferred nucleation sites are determined by the spatial structure of the unstable modes. Once those sites have nucleated, no new sites become available, and growth slows as field energy is consumed.

The slight increase in n in the recovery regime (0.690 vs 0.682 at the fundamental) suggests that at higher driving frequencies the nucleation sites are slightly less constrained, perhaps reflecting the broader k-space structure of higher harmonic resonance bands.

6.3 Implications

The correspondence between Floquet theory and Avrami kinetics has implications beyond the specific system studied here. Any physical system governed by parametric instability — including pattern formation in driven fluids, structure formation in modulated optical lattices, phonon-driven phase transitions in crystalline solids, and parametric amplification in driven quantum systems — may exhibit Avrami nucleation statistics whose exponents reflect the underlying Floquet band structure.

The identification of Avrami kinetics as a quantitative probe of Floquet band structure suggests a new experimental observable for systems where direct measurement of the Floquet spectrum is difficult. By measuring nucleation statistics and fitting the Avrami exponent, one can in principle infer properties of the parametric stability landscape without explicitly computing the monodromy matrix.

6.4 Conclusion

We have demonstrated that Floquet parametric resonance theory and Avrami nucleation kinetics are unified descriptions of frequency-locked phase transitions in driven scalar field systems. A systematic numerical sweep across eight harmonic multiples of the fundamental frequency $\omega_0 = 0.313$ reveals three distinct dynamical regimes whose boundaries correspond to features of the Floquet stability spectrum.

These results establish a formal bridge between two mathematical frameworks that have developed independently across different scientific domains. The Avrami exponent n emerges as a quantitative observable encoding Floquet band structure — a result with potential applications across any physical system governed by parametric instability and phase transition dynamics.

Acknowledgments

The author thanks Professor William G. Unruh (University of British Columbia) for correspondence regarding acoustic black hole analogs and their connection to the theoretical framework underlying this work. Simulations were performed on a Dell Precision 5540 workstation. This work was conducted under the auspices of Pax-Dualon Research Institute LLC, Logan, Utah, established in memory of Bryson Pax McKenna (March 28, 2009 — August 6, 2024).

References

[1] Floquet, G. (1883). Sur les équations différentielles linéaires à coefficients périodiques. Annales de l'École Normale Supérieure, 12, 47–88.

[2] Avrami, M. (1939). Kinetics of phase change I. Journal of Chemical Physics, 7, 1103–1112.

[3] Avrami, M. (1940). Kinetics of phase change II. Journal of Chemical Physics, 8, 212–224.

[4] Avrami, M. (1941). Kinetics of phase change III. Journal of Chemical Physics, 9, 177–184.

[5] Mathieu, É. (1868). Mémoire sur le mouvement vibratoire d'une membrane de forme elliptique. Journal de Mathématiques Pures et Appliquées, 13, 137–203.

[6] Hill, G.W. (1886). On the part of the motion of the lunar perigee. Acta Mathematica, 8, 1–36.

[7] Unruh, W.G. (1981). Experimental black hole evaporation? Physical Review Letters, 46, 1351–1353.

[8] Kofman, L., Linde, A., Starobinsky, A.A. (1997). Towards the theory of reheating after inflation. Physical Review D, 56, 3258–3295.

[9] Christian, J.W. (2002). The Theory of Transformations in Metals and Alloys. Pergamon Press, Oxford.

[10] Grimshaw, R. (1990). Nonlinear Ordinary Differential Equations. CRC Press.

Manuscript prepared for submission to Physical Review E